Large lattice thermal conductivity, interplay between phonon-phonon, phonon-electron, and phonon-isotope scatterings, and electrical transport in molybdenum from first principles

Shihao Wen,[1] Jinlong Ma,[1,2] Ashis Kundu,[1,3] and Wu Li[1,4,*]

[1]*Institute for Advanced Study, Shenzhen University, Shenzhen 518060, China*

[2]*School of Energy and Power Engineering, Huazhong University of Science and Technology, Wuhan 430074, China*

[3]*Key Laboratory of Optoelectronic Devices and Systems of Ministry of Education and Guangdong Province, College of Physics and Optoelectronic Engineering, Shenzhen University, Shenzhen 518060, China*

[4]*Center for Quantum Transport and Thermal Energy Science, School of Physics and Technology, Nanjing Normal University, Nanjing 210023, China*

(Received 11 February 2020; revised 11 June 2020; accepted 21 July 2020; published 5 August 2020)

We describe an *ab initio* phonon Boltzmann transport equation (BTE) approach accounting for phonon-electron scattering in addition to the well-established phonon-phonon and isotope scatterings. The phonon BTE is linearized and can be exactly solved beyond the relaxation time approximation (RTA). We use this approach to study the lattice thermal conductivity (κ_{ph}) of molybdenum (Mo). κ_{ph} of Mo is found to possess several anomalous features: (1) like in another group VI element tungsten (W), κ_{ph}, with a large value of 37 W m^{-1} K^{-1} at room temperature, follows weak temperature dependence due to interplay between phonon-phonon (ph-ph), phonon-electron (ph-el), and phonon-isotope (isotope) scatterings; and (2) compared with W, though Mo is much lighter in mass, Mo has a smaller κ_{ph}. This is attributed to weaker interatomic bonding, larger isotope mixture, and larger density of states at Fermi level in Mo. In isotopically pure samples, κ_{ph} increases from 37 to 48 W m^{-1} K^{-1} at room temperature. Considering the similarity of the phonon dispersion, our work suggests that chromium should also have a large κ_{ph}, which, rather than the complexity of the electronic band structure argued in the literature, accounts for the significant deviation of measured Lorenz number L from the expected Sommerfeld value. The electrical conductivity (σ) and electronic thermal conductivity (κ_e) of Mo are also calculated by using an *ab initio* electron BTE approach. σ and the total thermal conductivity (κ) agree with the experimental data reasonably. These results demonstrate that the *ab initio* calculations can quantify the lattice and electronic contributions to κ. We also look into the cumulative σ and κ_{ph} with respect to electron and phonon mean free paths (MFPs), respectively, in order to reveal the size effect in Mo. The MFPs of electrons contributing to conductivity range from 5 to 22 nm, whereas the MFPs of phonons primarily distribute between 5 and 73 nm with more than 80% contribution to κ_{ph}. This suggests that a reduced Lorenz number can be observed in Mo nanostructures when the relevant size goes below ~70 nm.

DOI: 10.1103/PhysRevB.102.064303

I. INTRODUCTION

In crystalline materials, the heat is conducted by electrons and phonons (lattice). Generally, for nonmetallic systems, the thermal conductivity is mainly contributed by phonons, while for metallic systems it is dominated by electrons. According to the Wiedemann-Franz law, the electronic thermal conductivity divided by the electrical conductivity (σ) and the temperature (T) is a universal constant, known as the Lorenz number L. Considering that L measured with the total thermal conductivity agrees with the theoretical Sommerfeld value $L_0 = \pi^2 k_B^2/3e^2 = 2.44 \times 10^{-8}$ W Ω K^{-2} within a few percentages in many metals, it was conventionally thought that the lattice has a negligible contribution in metals. However, recently a few transition metal carbides [1,2] and elemental tungsten [3] have been identified to be exceptions. Specifically κ_{ph} reaches as much as 46 W m^{-1} K^{-1} in tungsten [3], comparable to common semiconductors like Ge and accounting for deviation of L from L_0.

Interestingly in some of those metals with large κ_{ph} such as group-V and group-VI carbides [1,2], and elemental W [3], the ph-el coupling also plays an important role in the phonon scattering. The interplay between temperature-independent ph-el and the temperature-dependent ph-ph scatterings leads to the anomalously weak temperature dependence of κ_{ph} [1–3], and signifies the increasing importance of an accurate solution to the Boltzmann transport equation beyond the relaxation time approximation as the temperature increases [3]. The key to the interplay is weak ph-el scattering and strong ph-ph scattering. In the case of group-V carbides and the group-VI carbide WC, the weak ph-ph scattering is associated with the large frequency gaps between acoustic and optic phonons [1,2], which has its origin in the electronic structure [2]. In the case of W, the overall weak ph-ph scattering is facilitated with the strong interatomic bonding [3]. Moreover, the weak ph-ph scattering, particularly at intermediate frequencies, is attributed to the elemental bcc

*wu.li.phys2011@gmail.com

structure [4]. The triple degeneracy at P and H points leads to vanishing scattering at those points. It was also found that in other elemental bcc systems like Na, the ph-ph scattering is strong due to the unusually soft transverse acoustic phonon along the Γ-N direction [4].

In this work, we present the derivation of linearized phonon BTE accounting for ph-el scattering in addition to the well-established ph-ph and isotope scatterings. We then quantify the lattice and electronic contribution to the thermal conductivity in elemental Mo from first-principles calculations. Due to features in the phonon dispersion similar to W, its $\kappa_{\rm ph}$ also possesses anomalous features including large value and weak temperature dependence. In addition, we find that the isotope scattering also plays an important role. In isotopically pure samples, $\kappa_{\rm ph}$ increases from 37 to 48 W m^{-1} K^{-1} at room temperature. We also study electrical conductivity and electronic thermal conductivity from the first principles. Reasonable agreement with experimental data is found. We also look into the mean free path (MFP) distributions of electrons and phonons, closely relevant to the size effects in nanostructures.

II. METHODOLOGY

A. Boltzmann transport equation

Lattice thermal conductivity can be calculated by solving the Boltzmann transport equation. At steady state, the changes of phonon occupation numbers n due to diffusion arising from the temperature gradient ∇T and the scattering need to balance out,

$$\frac{\partial n_\lambda}{\partial t} = \left.\frac{\partial n_\lambda}{\partial t}\right|_{\rm diff} + \left.\frac{\partial n_\lambda}{\partial t}\right|_{\rm scatt} \equiv 0, \tag{1}$$

where λ is a composite index comprising both wave vector $\mathbf{q}$ and branch index p. Keeping linear terms with ∇T, the diffusion term can be expressed as

$$\left.\frac{\partial n_\lambda}{\partial t}\right|_{\rm diff} = -\frac{\partial n_\lambda}{\partial T}\nabla T\cdot\mathbf{v}_\lambda \approx -\frac{\hbar\omega_\lambda}{k_B T^2} n_\lambda^0\left(1+n_\lambda^0\right)\nabla T\cdot\mathbf{v}_\lambda, \tag{2}$$

where n_λ^0 and $\mathbf{v}_\lambda$ are the equilibrium Bose-Einstein distribution and velocity for phonon λ, respectively.

It is convenient to write the equation in terms of the deviation of n_λ from n_λ^0, defined as $\chi_\lambda = n_\lambda - n_\lambda^0$ and keeping only the linear terms with χ_λ in the scattering term, since the zeroth-order terms corresponding to the equilibrium state do not change n_λ. The scattering mechanisms depend on the system. In metals, the intrinsic mechanisms include anharmonic ph-ph, isotope, and ph-el scatterings. The scattering rate for individual process needs to account for the actual occupation numbers. Hereafter we use Γ to denote the actual scattering rate at equilibrium.

Any scattering process annihilating one phonon in the state λ has a factor n_λ involved in the actual transition rate, while its reverse process creating one phonon in the state λ involves a factor $(1+n_\lambda)$. Due to the two reversible processes, the change of n_λ contributes to $\partial n_\lambda/\partial t$ a term proportional to Γ_λ with a prefactor $-\chi_\lambda/n_\lambda^0 + \chi_\lambda/(1+n_\lambda^0)$. If writing $\chi_\lambda = n_\lambda^0(1+n_\lambda^0)\Psi_\lambda$, the prefactor becomes $-(1+n_\lambda^0)\Psi_\lambda + n_\lambda^0\Psi_\lambda = -\Psi_\lambda$, where Ψ_λ can be regarded as a small perturbation.

Ph-el scattering is a process involving only one phonon. Regarding isotope scattering, an elastic two-phonon process, annihilating one phonon in the state λ will simultaneously create one phonon λ'. The reverse process annihilates λ' and creates one phonon λ. Apart from the $-\Psi_\lambda$ contribution from the change of n_λ, the change of $n_{\lambda'}$ contributes to $\partial n_\lambda/\partial t$ a term proportional to $\Gamma^{\rm isotope}_{\lambda\lambda'}$ with a prefactor $\Psi_{\lambda'}$.

This rule can be easily extended to multiple-phonon scattering processes. For instance, in anharmonic three-phonon processes, the scattering process annihilating one phonon in the state λ involves creation of some phonon λ'' plus annihilation (creation) of another phonon λ', denoted as $+$ $(-)$ process. Apart from the contribution from the change of n_λ and $n_{\lambda''}$, the change of $n_{\lambda'}$ contributes to $\partial n_\lambda/\partial t$ a prefactor $-\Psi_{\lambda'}$ $(\Psi_{\lambda'})$.

Thus considering the three intrinsic mechanisms, we have

$$\begin{aligned}\left.\frac{\partial n_\lambda}{\partial t}\right|_{\rm scatt} = & -\Gamma^{\text{ph-el}}_\lambda\Psi_\lambda - \sum_{\lambda'}\Gamma^{\rm isotope}_{\lambda\lambda'}(\Psi_\lambda - \Psi_{\lambda'}) \\ & - \frac{1}{N_{\mathbf{q}}}\sum_{\lambda'\lambda''}^{+}\Gamma^{+}_{\lambda\lambda'\lambda''}(\Psi_\lambda + \Psi_{\lambda'} - \Psi_{\lambda''}) \\ & - \frac{1}{2}\frac{1}{N_{\mathbf{q}}}\sum_{\lambda'\lambda''}^{-}\Gamma^{-}_{\lambda\lambda'\lambda''}(\Psi_\lambda - \Psi_{\lambda'} - \Psi_{\lambda''}),\end{aligned} \tag{3}$$

where $\Gamma^{\text{ph-el}}_\lambda$ has already accounted for all possible ph-el scattering processes for simplicity, $N_{\mathbf{q}}$ is the number of uniformly sampled $\mathbf{q}$ points, and $\frac{1}{2}$ is due to double-counting in the sum for the $-$ processes. Additionally, the quasimomentum conservation requires $\mathbf{q}'' = \mathbf{q}\pm\mathbf{q}+\mathbf{G}$ in the sum for the $+$ and $-$ processes, respectively, where $\mathbf{G}$ is a reciprocal lattice vector, and is zero for momentum-conserving normal processes and nonzero for resistive Umklapp processes.

Since $\frac{\partial n_\lambda}{\partial t}|_{\rm diff}$ contains a common factor $-\frac{\hbar}{k_B T^2}\nabla T$, it is convenient to further write $\Psi_\lambda = -\frac{\hbar}{k_B T^2}\nabla T\cdot\mathbf{E}_\lambda$ and introduce $\bar\Gamma_\lambda = \Gamma_\lambda/[n_\lambda^0(1+n_\lambda^0)]$, then Eq. (1) is linearized in terms of $\mathbf{E}_\lambda$:

$$\mathbf{E}_\lambda = \omega_\lambda\tau_\lambda\mathbf{v}_\lambda + \tau_\lambda\mathbf{\Delta}_\lambda. \tag{4}$$

$$\begin{aligned}\mathbf{\Delta}_\lambda = & \frac{1}{N_{\mathbf{q}}}\sum_{\lambda'\lambda''}^{+}\bar\Gamma^{+}_{\lambda\lambda'\lambda''}(\mathbf{E}_{\lambda''} - \mathbf{E}_{\lambda'}) \\ & + \frac{1}{2N_{\mathbf{q}}}\sum_{\lambda'\lambda''}^{-}\bar\Gamma^{-}_{\lambda\lambda'\lambda''}(\mathbf{E}_{\lambda''} + \mathbf{E}_{\lambda'}) + \frac{1}{N_{\mathbf{q}}}\sum_{\lambda'}\bar\Gamma^{\rm isotope}_{\lambda\lambda'}\mathbf{E}_{\lambda'}.\end{aligned} \tag{5}$$

The expression for $\mathbf{\Delta}_\lambda$ remains the same as the case without including ph-el scattering, due to the fact that each ph-el scattering process involves one phonon only. The total relaxation

time τ_λ needs to account for all scattering:

$$\begin{aligned}\frac{1}{\tau_\lambda} &= \frac{1}{\tau_\lambda^{\text{ph-ph}}} + \frac{1}{\tau_\lambda^{\text{isotope}}} + \frac{1}{\tau_\lambda^{\text{ph-el}}} \\ &= \left[\frac{1}{N_\mathbf{q}}\sum_{\lambda'\lambda''}^{+}\bar{\Gamma}^{+}_{\lambda\lambda'\lambda''} + \frac{1}{2N_\mathbf{q}}\sum_{\lambda'\lambda''}^{-}\bar{\Gamma}^{-}_{\lambda\lambda'\lambda''}\right] \\ &\quad + \frac{1}{N_\mathbf{q}}\sum_{\lambda'}\bar{\Gamma}^{\text{isotope}}_{\lambda\lambda'} + \bar{\Gamma}^{\text{ph-el}}_{\lambda},\end{aligned} \tag{6}$$

$\mathbf{E}_\lambda$ can be accurately solved using an iterative method starting with the zero-order RTA solution $\mathbf{E}^0_\lambda \equiv \mathbf{E}^{\text{RTA}}_\lambda = \omega_\lambda\tau_\lambda\mathbf{v}_\lambda$ [5]. Alternatively, $\mathbf{E}_\lambda/\omega_\lambda$ can be solved iteratively. We note that RTA was employed in the literature [6–12]. With calculated $\mathbf{E}_\lambda$, the lattice thermal conductivity can be obtained as [5]

$$\kappa_{\text{ph}} = \frac{1}{N_\mathbf{q}Vk_BT^2}\sum_\lambda n^0_\lambda\left(n^0_\lambda+1\right)\hbar^2\omega_\lambda\mathbf{v}_\lambda\otimes\mathbf{E}_\lambda. \tag{7}$$

B. Phonon-phonon scattering

For the + and − processes, the energy conservation condition requires $\omega_\lambda+\omega_{\lambda'}=\omega_{\lambda''}$ and $\omega_\lambda-\omega_{\lambda'}=\omega_{\lambda''}$, leading to $n^0_\lambda n^0_{\lambda'}(1+n^0_{\lambda''}) = n^0_\lambda(1+n^0_\lambda)(n^0_{\lambda'}-n^0_{\lambda''})$ and $n^0_\lambda(1+n^0_{\lambda'})(1+n^0_{\lambda''}) = n^0_\lambda(1+n^0_\lambda)(1+n^0_{\lambda'}+n^0_{\lambda''})$, respectively. Thus it follows that

$$\bar{\Gamma}^{+}_{\lambda\lambda'\lambda''} = \frac{h}{8}|V^{+}_{\lambda\lambda'\lambda''}|^2\left(n^0_{\lambda'}-n^0_{\lambda''}\right)\frac{\delta(\omega_\lambda+\omega_{\lambda'}-\omega_{\lambda''})}{\omega_{\lambda'}\omega_{\lambda'}\omega_{\lambda''}}, \tag{8}$$

$$\bar{\Gamma}^{-}_{\lambda\lambda'\lambda''} = \frac{h}{8}|V^{-}_{\lambda\lambda'\lambda''}|^2\left(n^0_{\lambda'}+n^0_{\lambda''}+1\right)\frac{\delta(\omega_\lambda-\omega_{\lambda'}-\omega_{\lambda''})}{\omega_{\lambda'}\omega_{\lambda'}\omega_{\lambda''}}, \tag{9}$$

where $V^{\pm}_{\lambda\lambda'\lambda''}$ are [13,14]

$$V^{\pm}_{\lambda\lambda'\lambda''} = \sum_{i\in u.c.}\sum_{j,k}\sum_{\alpha\beta\gamma}\Phi^{\alpha\beta\gamma}_{ijk}\frac{e^\alpha_\lambda(i)e^\beta_{\pm\lambda'}(j)e^\gamma_{-\lambda}(k)}{\sqrt{M_iM_jM_k}}, \tag{10}$$

where u.c. is short for unit cell, M stands for the mass of each atom, $\Phi^{\alpha\beta\gamma}_{ijk}$ are the third-order force constants, and e_λ is the normalized eigenvector.

C. Isotope scattering

The isotope scattering is an elastic process, thus the isotope scattering rate $\bar{\Gamma}^{\text{isotope}}_{\lambda\lambda'}$ is independent of the phonon occupation numbers, and given by [15]

$$\bar{\Gamma}^{\text{isotope}}_{\lambda\lambda'} = \frac{\pi\omega^2}{2}\sum_{i\in u.c.}g(i)|e^*_\lambda\cdot e_{\lambda'}(i)|^2\delta(\omega_\lambda-\omega_{\lambda'}), \tag{11}$$

in which $g(i)=\sum_s f_s[1-M_s(i)/\overline{M}(i)]^2$ is the Pearson deviation coefficient. $M_s(i)$ is the sth isotopes of the ith atom with a probability distribution f_s. $\overline{M}(i)$ is the expectation of $M_s(i)$. For Mo with natural abundance, $g=5.98\times10^{-4}$. In comparison, $g=6.97\times10^{-5}$ for W, about one order of magnitude smaller due to a smaller isotope mixture.

D. Phonon-electron scattering

In ph-el scattering, an electron in state $|n\mathbf{k}\rangle$ scatter into one state $|m\mathbf{k}+\mathbf{q}\rangle$ by annihilating one phonon λ. The energy conservation condition requires $E_{n\mathbf{k}}+\hbar\omega_\lambda = E_{m\mathbf{k}+\mathbf{q}}$, leading to $f^0_{n\mathbf{k}}n^0_\lambda(1-f^0_{m\mathbf{k}+\mathbf{q}}) = n^0_\lambda(1+n^0_\lambda)(f^0_{n\mathbf{k}}-f^0_{m\mathbf{k}+\mathbf{q}})$. It follows that

$$\begin{aligned}\bar{\Gamma}^{\text{ph-el}}_\lambda &= \frac{2\pi}{\hbar}\frac{2}{N_\mathbf{k}}\sum_{mn\mathbf{k}}\left|g^{m\mathbf{k}+\mathbf{q}}_{n\mathbf{k},\lambda}\right|^2\left(f^0_{n\mathbf{k}}-f^0_{m\mathbf{k}+\mathbf{q}}\right) \\ &\quad\times\delta(E_{m\mathbf{k}+\mathbf{q}}+\hbar\omega_\lambda-E_{n\mathbf{k}}) \\ &\approx 2\pi\omega_{\mathbf{q}p}\frac{2}{N_\mathbf{k}}\sum_{mn\mathbf{k}}\left|g^{m\mathbf{k}+\mathbf{q}}_{n\mathbf{k},\mathbf{q}p}\right|^2\delta(E_{m\mathbf{k}+\mathbf{q}}-E_f)\delta(E_{n\mathbf{k}}-E_f),\end{aligned} \tag{12}$$

where $N_\mathbf{k}$ is the number of uniformly sampled $\mathbf{k}$ points, the factor 2 in $2/N_\mathbf{k}$ accounts for the spin degeneracy in spin-unpolarized calculations, and E_f is the Fermi level. $|g^{m\mathbf{k}+\mathbf{q}}_{n\mathbf{k},\lambda}|$ here is the corresponding electron-phonon coupling matrix, which can be calculated from the first-principle calculation [3]. As is manifested in Eq. (12), the ph-el scattering can be regarded as temperature-independent.

E. Electrical conductivity and electronic thermal conductivity

We can also employ electron BTE to calculate the electrical conductivity σ as [16]

$$\sigma^{\alpha\beta} = \frac{2e^2}{N_\mathbf{k}Vk_BT}\sum_{n\mathbf{k}}f^0_{n\mathbf{k}}\left(1-f^0_{n\mathbf{k}}\right)\mathbf{v}^\alpha_{n\mathbf{k}}\mathbf{F}^\beta_{n\mathbf{k}}, \tag{13}$$

where $\mathbf{F}_{n\mathbf{k}}$ can be regarded as the mean free displacement of electron in state $n\mathbf{k}$. Meanwhile, BTE can be applied to obtain the electronic thermal conductivity κ_{e} as [17]

$$\begin{aligned}\kappa_{\text{e}} &= \frac{2}{N_\mathbf{k}Vk_BT^2}\sum_{n\mathbf{k}}f^0_{n\mathbf{k}}\left(1-f^0_{n\mathbf{k}}\right)(E_{n\mathbf{k}}-E_f)^2\mathbf{v}_{n\mathbf{k}} \\ &\quad\otimes\mathbf{F}_{n\mathbf{k}} - T\sigma S^2,\end{aligned} \tag{14}$$

where

$$\sigma S = \frac{2e}{N_\mathbf{k}Vk_BT^2}\sum_{n\mathbf{k}}f^0_{n\mathbf{k}}\left(1-f^0_{n\mathbf{k}}\right)(E_{n\mathbf{k}}-E_f)\mathbf{v}_{n\mathbf{k}}\otimes\mathbf{F}_{n\mathbf{k}}. \tag{15}$$

BTE can also be approximately solved with RTA [16,18–21], momentum RTA (MRTA) [16], and Allen's formula [22]. An efficiency factor α_{tr} weighing the contribution of scattering with the relative change of velocity:

$$\alpha_{\text{tr}} = 1-\frac{\mathbf{v}_{m\mathbf{k}+\mathbf{q}}\cdot\mathbf{v}_{n\mathbf{k}}}{|\mathbf{v}_{n\mathbf{k}}|^2}, \tag{16}$$

is considered in the latter two cases. The transport spectral function α^2F_{tr} in Allen's approximation can be found from Eliashberg ph-el spectral function α^2F [16,22]:

$$\alpha^2F(\omega) = \frac{1}{4\pi N_\mathbf{q}N_F}\sum_\lambda\frac{\bar{\Gamma}^{\text{ph-el}}_\lambda}{\omega_\lambda}\delta(\omega-\omega_\lambda), \tag{17}$$

by multiplying the term in the sum of Eq. (12) by α_{tr}. It can be used to obtain electrical resistivity ρ:

$$\rho(T) = \frac{2\pi Vk_BT}{e^2\hbar N_F\langle v_z^2\rangle}\int_0^\infty\frac{\alpha^2F_{\text{tr}}(\omega)d\omega}{\omega}\frac{x^2}{\sinh^2x}, \tag{18}$$

where N_F is the electron density of states per unit cell and spin at Fermi level E_f. $\langle v_z^2\rangle$ is the expectation square of the

Fermi velocity in the transport direction. Thus a total coupling constant λ can be defined as

$$\lambda = \frac{1}{N_{\mathbf{q}}} \sum_{\lambda} \frac{\bar{\Gamma}_{\lambda}^{\text{ph-el}}}{2\pi N_F \omega_{\lambda}^2} = 2 \int \frac{\alpha^2 F(\omega)}{\omega} d\omega. \tag{19}$$

There also exists a variant λ_{tr} corresponding to $\alpha^2 F_{\text{tr}}$.

F. Computational method

The electron energy, phonon frequency, ph-el coupling matrix were calculated with the QUANTUM ESPRESSO package [24], using density functional theory (DFT) and density functional perturbation theory. The Trouiller-Martins type norm-conserving pseudopotentials [25] under generalized-gradient approximation with Perdew-Burke-Ernzerhof parametrization [26] and the local density approximation with Perdew-Wang parametrization [27] were used. The EPW package [28] was used to perform Wannier interpolation for electron-phonon coupling matrix. Initial **k** and **q** grids are $8 \times 8 \times 8$ while final **k** and **q** grids are $100 \times 100 \times 100$ for electron-phonon and $32 \times 32 \times 32$ for ph-el scatterings. VASP [29,30] and thirdorder.py in the SHENGBTE [31–33] package were used to perform third-order interatomic force constants (IFCs) with a cutoff of the sixth nearest neighbor. SHENGBTE package [31–33] was further used to calculate κ_{ph} with and without considering ph-el scattering. We did a convergence test to show that a large **q** and **k** grid is necessary for electric conductivity σ and electronic thermal conductivity κ_{e}.

The energy-resolved visualization of chemical bonding was executed by calculating the crystal orbital Hamiltonian population (COHP) [34] as implemented in the LOBSTER package [35].

III. RESULT

A. Phonon dispersions

Figure 1 shows the calculated phonon dispersions of Mo along high symmetry directions in the Brillouin zone. In order to see the effect of exchange-correlation functionals, the phonon dispersions are calculated using both LDA and PBE. The PBE results show better agreement with the experiment. The LDA results are slightly higher due to its well-known overbinding. The phonon frequencies are triply degenerate at P and H points, which is attributed to the space group symmetry of elemental bcc structure [4]. Compared with another group VI element W, the atomic mass of Mo is nearly half of W, but the phonon frequencies of Mo are only slightly higher [3]. This suggests that Mo has a weaker bonding than W. To understand the bonding, we show the DOS along with COHP and Integrated-COHP (ICOHP) for the nearest-neighbor atom in Fig. 2. COHP is a quantitative way to analyze bonding. A negative COHP corresponds to bonding interaction and lowers the system energy, whereas a positive COHP corresponds to antibonding interaction and enhances the system energy [34]. From COHP, it can be seen that for both Mo and W the bonding and antibonding states are separated at the Fermi energy, around which the DOS is locally minimized. The larger ICOHP at the Fermi energy

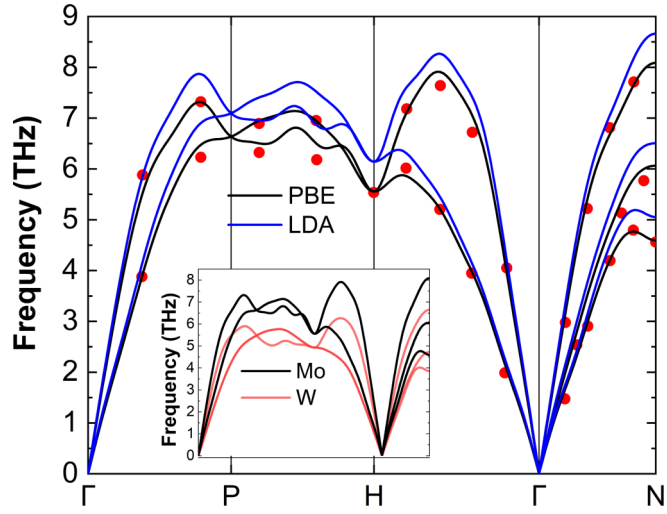

FIG. 1. Calculated phonon dispersion along high-symmetry directions for Mo. Solid circles represent experimental results taken from Ref. [23]. A comparison of phonon dispersion between Mo (PBE) and W is shown in the inset.

for W reveals the relatively stronger covalency than that of Mo [36]. Actually, the 5*d* orbitals for W are more extended and can overlap more effectively than 4*d* orbitals for Mo, thus leading to stronger covalency.

B. Lattice thermal conductivity

The calculated κ_{ph} using PBE and LDA is shown in Fig. 3(a) for Mo. The LDA κ_{ph} is 26% higher than the PBE value when ph-el interaction is not considered. However, the difference reduces to about 7% when ph-el interaction is considered. This difference in κ_{ph} between LDA and PBE can be understood from the higher LDA phonon frequencies than PBE, leading to smaller ph-ph scattering rates in addition to

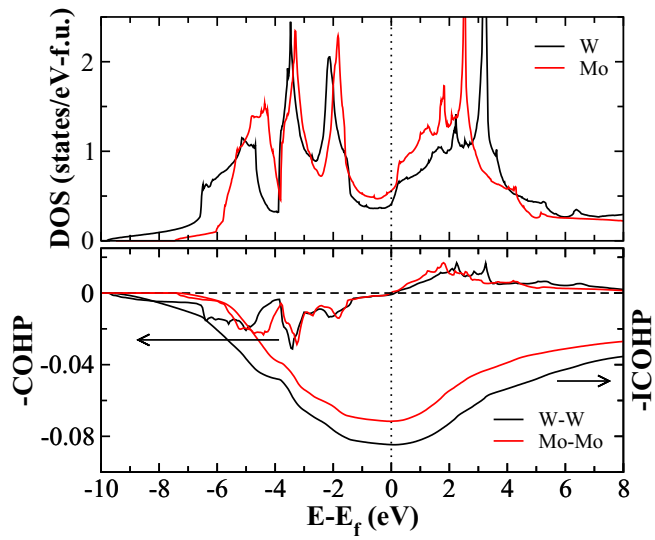

FIG. 2. Calculated density of states (DOS), and COHP and ICOHP vs energy with respect to the Fermi energy (E_f) for W and Mo.

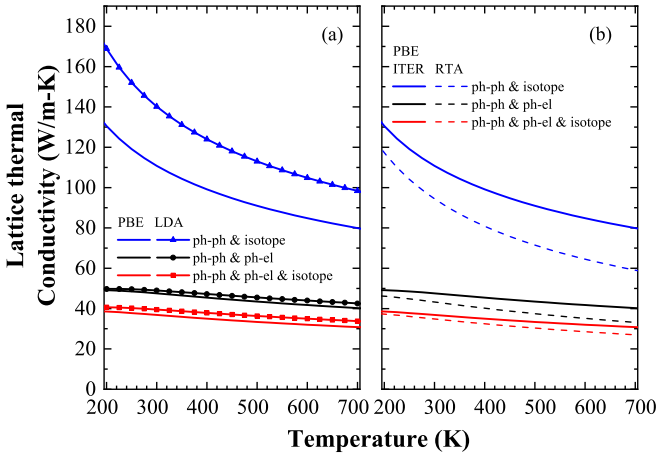

FIG. 3. Calculated lattice thermal conductivity (κ_{ph}) for Mo limited by different combination of ph-ph, ph-el, and isotope interactions. (a) comparison of κ_{ph} calculated using PBE and LDA. (b) Comparison of κ_{ph} obtained from iterative solution (solid lines) and RTA (dashed lines) of BTE using PBE.

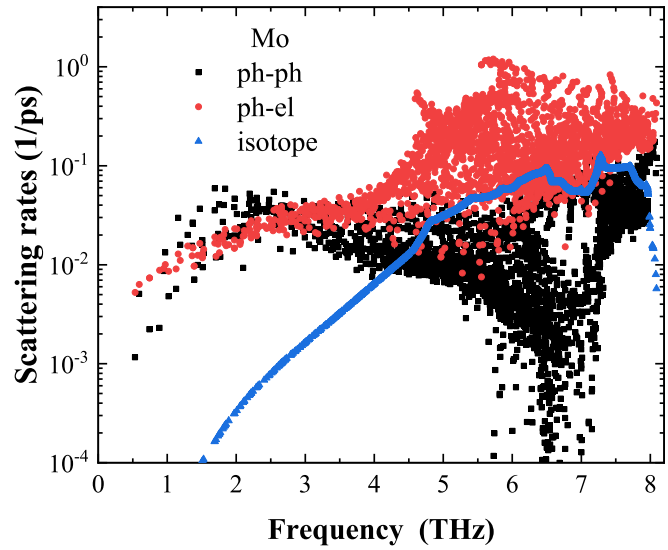

FIG. 4. Calculated ph-ph, ph-el and isotope scattering rates for Mo at 300 K.

larger group velocities in LDA [37]. Despite the difference in κ_{ph}, we will concentrate on the results obtained by using PBE hereafter as the calculated phonon dispersion matches better with the experimental values.

The value of κ_{ph} limited by ph-ph, ph-el and isotope scatterings combined, reaches 37 W m^{-1} K^{-1} at 300 K (Fig. 3). For systems consisting of atoms of the same group of the periodic table, usually those with heavier elements have lower κ_{ph}. However it is smaller than that for W (46 W m^{-1} K^{-1}) [3]. Nevertheless, it is still much larger than those of other elemental metals such as Al (6 W m^{-1} K^{-1}), Ag (4 W m^{-1} K^{-1}), and Au (2 W m^{-1} K^{-1}) [7]. Like in group-V and group-VI carbides [1,2], and elemental W [3], κ_{ph} displays anomalously weak temperature dependence. Specifically, κ_{ph} decreases from 38 W m^{-1} K^{-1} at 200 K to 31 W m^{-1} K^{-1} at 700 K, by only 18%. In contrast, κ_{ph} typically follows $1/T$ dependence around and above the Debye temperature.

To analyze the underlying mechanism for the large κ_{ph} and the weak temperature dependence, we plot the ph-ph, ph-el, and isotope scattering rates in Fig. 4. The ph-ph scattering rates are the smallest at intermediate frequencies. It is the weak ph-ph scattering that leads to the large κ_{ph}. The ph-ph scattering rates of Mo are similar to W [3]. The weaker bonding in Mo leads to larger thermal displacement, suggesting stronger ph-ph scattering. However, it is canceled out by the weaker anharmonicity in the interatomic potential, characterized by the third-order IFCs. We look into the third-order IFCs, and find that the third-order IFCs in Mo are smaller than those in W by about 30%. The weak nature of the scattering rates at intermediate frequencies are closely related to triple degeneracy at P and H points and thus the elemental bcc structure [4]. Due to the triple degeneracy and the nearly isotropic feature of the phonon dispersions at long wavelengths, the three-phonon scattering channels are completely closed, and therefore the ph-ph scattering rates vanish at those points. Though ph-el scatterings in Mo are weaker than many other metals [3,7], the much weaker ph-ph scatterings, particularly those at intermediate frequencies, lead to a predominance of ph-el scatterings. Correspondingly, κ_{ph} is tripled to 111 W m^{-1} K^{-1} at 300 K when the ph-el scattering is excluded. The temperature-independent ph-el scattering explains the weak temperature dependence of κ_{ph}. As compared to W, the ph-el scatterings of Mo are slightly larger. If replacing the ph-el scattering rates of Mo with those of W for phonons with the same wavevectors, the calculated κ_{ph} can be slightly increased from 37 W m^{-1} K^{-1} by 10%. The larger ph-el scatterings in Mo is related to larger DOS at the Fermi level (Fig. 2), which allows for more scattering channels.

Interestingly, in contrast to W, where the isotope scattering is almost negligible, the isotope scattering in Mo also plays an important role. Due to large isotope mixture, as reflected by the g factor in Eq. (11), the isotope scatterings are almost one order of magnitude larger than those for W. In isotopically pure Mo samples, where the isotope scatterings are absent, κ_{ph} increases by almost 30% as shown in Fig. 3. For instance, at room temperature, κ_{ph} becomes 48 W m^{-1} K^{-1}. The isotope enhancement effect of κ_{ph} is comparable to diamond [38].

To look further into the scattering, we show the comparison with RTA results of κ_{ph} in Fig. 3(b). In the case of only ph-ph and isotope scatterings included, RTA apparently underestimates the results, and the relative underestimate increases from 10% at 200K to 26% at 700 K. Normal three-phonon processes conserve phonon momentum, and thus do not resist heat flow directly. In contrast, Umklapp processes do not conserve momentum, and therefore pose direct resistance to phonon transport [39]. However, in RTA, both Umklapp and normal three-phonon processes are considered equally resistive, and thus RTA underestimates κ_{ph}. This large underestimate also suggests the normal processes account for a large portion of three-phonon scattering processes. The completely resistive isotope scattering is temperature-independent, and the ph-ph scattering increases with temperature. As a result, the relative importance of normal processes increases

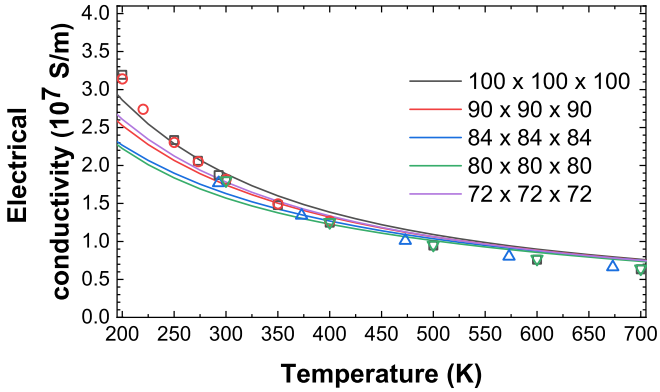

FIG. 5. The variation of electrical conductivity (σ) with temperature for several different grids of **k** and **q** samplings. **k** and **q** grids are kept the same for a given calculation. Symbols represent experimental results taken from Refs. [43,44].

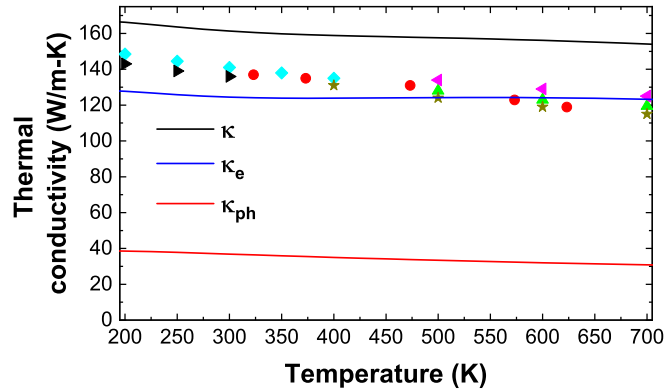

FIG. 6. The variation of calculated phonon thermal conductivity (κ_{ph}), electronic thermal conductivity (κ_{el}) and the total thermal conductivity ($\kappa = \kappa_{ph} + \kappa_{el}$). The symbols show experimental thermal conductivity taken from Ref. [45].

with temperature, leading to increasing underestimation of RTA. The ph-el scattering is also completely resistive and stronger than the isotope scattering. When ph-el scattering is considered, the underestimate by RTA becomes weaker. In the case where all the three types of phonon scatterings are included, RTA underestimates by 3% at 200K and by 12% at 700 K.

As aforementioned, in W and Mo, the triple degeneracy and the nearly isotropic feature of the phonon dispersions lead to the small ph-ph scattering at intermediate frequencies, which is crucial for the large value of κ_{ph} and the interplay with the ph-el scattering. We note that for another group VI element chromium, the measured phonon dispersions also display these features [40]. The mass difference between Cr and Mo is inadequate to account for the difference in the magnitude of corresponding phonon dispersions, and suggests that the interatomic bonding of Cr is only a bit weaker than Mo. Further, the g factor for the isotope mixture of Cr is smaller than that for Mo by a factor of about 5. These factors suggest that Cr could also have a large κ_{ph}. We do not manage to study Cr to confirm this, due to the fact that the DFT calculations for the antiferromagnetic systems such as Cr are much more involved. Actually, the measured L is larger than the Sommerfeld value by 50% at room temperature, which was argued to be due to the complexity of the electronic band structure [41,42]. We believe that the deviation of L should be attributed to the large lattice component of the measure thermal conductivity.

C. Electrical conductivity and electronic thermal conductivity

We have also studied the electrical transport properties of Mo. Figure 5 shows the convergence test of electrical conductivity (σ) with respect to **k** and **q** grids. The experimental data are also shown in Fig. 5 for comparison. At high temperatures (above 400 K), the calculated σ is well converged with respect to **k** and **q** grids and overestimated by 16% as compared to the experimental results. The discrepancy between calculated and experimental results at high temperatures might be due to the unconsidered temperature effects on phonon dispersion and electronic band structure. The overestimation in the calculated σ at high temperatures also observed for W and Al [3,46]. On the other hand, the calculated σ at low temperatures is not well converged, as it needs denser **k** and **q** grids, which are however beyond our computational capacities.

The electronic contribution to the thermal conductivity (κ_e) calculated with $100 \times 100 \times 100$ grids and the resulting total κ is plotted in Fig. 6, in comparison with the experiments. κ_e is almost temperature-independent, between 124 and 129 W m^{-1} K^{-1}. According to calculated σ and κ_e, within the whole temperature range, the electronic Lorenz number L_e is almost constantly 2.275×10^{-8} Ω K^{-2}, smaller than the Sommerfeld value L_0 by 7%. After adding the lattice contribution, the total κ is apparently higher than the experiments. Our calculated results overestimate the experimental values in the whole temperature range by 12-23%. At high temperatures, the overestimate of κ is mainly due to overestimated σ. The 16% overestimation in σ at 700 K causes κ_e to be overestimated by around 17 W m^{-1} K^{-1} if assuming L_e unaffected. Thus κ_e is not adequate to fully account for the measured total thermal conductivity, and there is a significant contribution

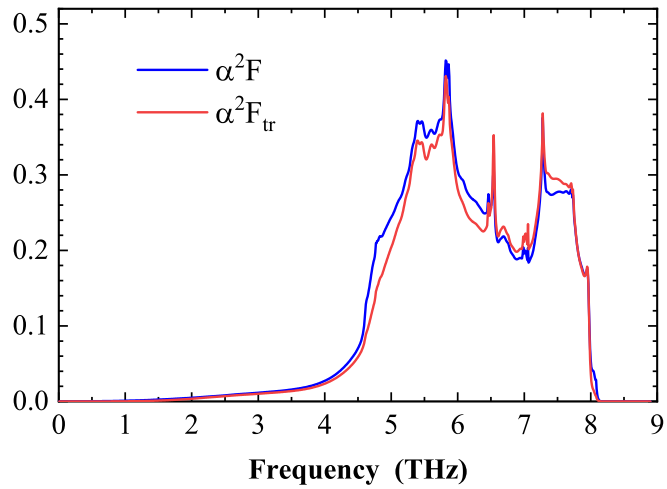

FIG. 7. The Eliashberg (α^2F) and transport (α^2F_{tr}) spectral function for Mo.

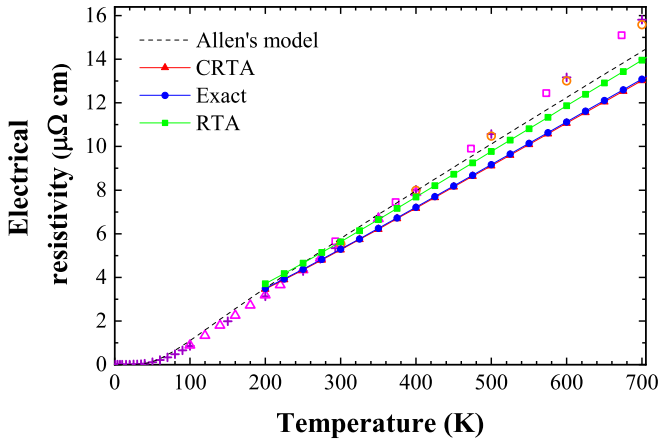

FIG. 8. Electrical resistivity as a function of temperature for Mo. The resistivity is calculated from Allen's Model as well as from the exact solution of BTE. The experimental results are taken from Ref. [43] (plus symbols) and Ref. [44] (the other symbols).

from $\kappa_{\rm ph}$. Considering the insufficient convergence at lower temperatures, the theoretical κ could be even higher. Actually, any defects in the samples can reduce κ below the theoretical value corresponding to the intrinsic upper limit, especially at low temperatures.

The calculated Eliashberg electron-phonon spectral function α^2F and its transport variant $\alpha^2F_{\rm tr}$ are shown in Fig. 7 for Mo. The corresponding values of electron-phonon coupling constant λ and its transport analog $\lambda_{\rm tr}$ are 0.33 and 0.31, respectively. The resistivity obtained from Eq. (18) is shown in Fig. 8. Allen's approximation slightly overestimates (underestimates) the experiment results below (above) 300 K. At high temperatures, it seems that Allen's approximation agrees better with experiments than the exact solution of BTE does. However, it is a coincidence, since the exact solution is well converged at high temperatures. As compared to the exact solution, RTA slightly overestimates. MRTA agrees excellently with the exact solution. It should be noted that

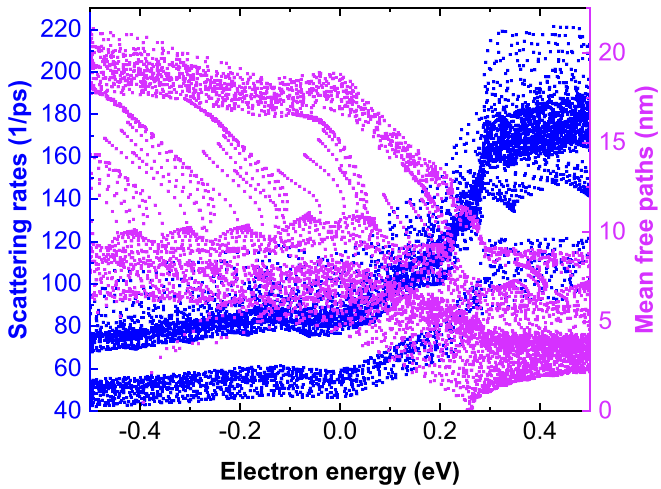

FIG. 9. Electron scattering rates and mean free paths vs energy with respect to the Fermi energy for Mo.

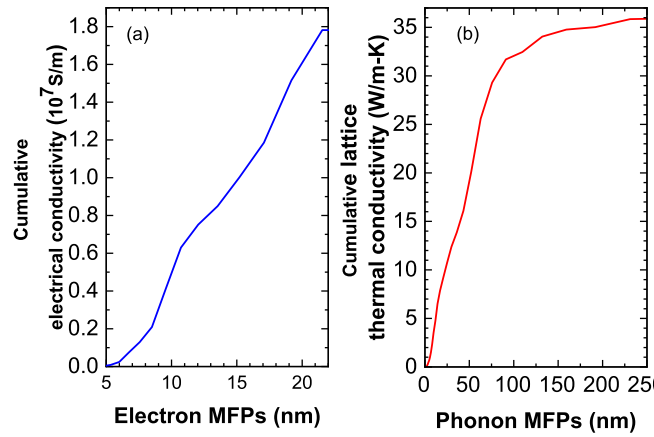

FIG. 10. Cumulative (a) electrical conductivity (σ) and (b) phonon thermal conductivity ($\kappa_{\rm ph}$) as a function of electron MFP and phonon MFP respectively, at 300 K.

MRTA loses its accuracy in the strongly anisotropic scattering cases like GaAs [20].

D. Electron and phonon MFPs

Figure 9 shows the scattering rates and mean free paths for electron. According to Allen's approximation, the average electron scattering rate above Debye temperature can be expressed as [22]

$$\overline{\tau^{-1}} = \frac{2\pi}{\hbar} k_B T \lambda_{\rm tr}. \tag{20}$$

The value for Mo is 76 ps^{-1} at 300 K, in consistent with the middle of the actual scattering rates at the Fermi energy, as shown in Fig. 9. This corresponds to an average lifetime of 13 fs, which is in good agreement with the value 12 fs estimated from experiment metal resistivity and calculated band structure [47].

Considering the size effect is relevant in applications of metal wires such as interconnect, we also show the electron's MFPs in Fig. 9. The MFP ranges from 5 to 19 nm at the Fermi energy. This supports the previous estimate of 11 nm in Ref. [47] for the average MFP. According to Fig. 10(a), electrons with MFPs from 5 to 21 nm contributes to the σ while 50% of σ is contributed by electrons with MFPs shorter than 14 nm.

Unlike electrons, phonons have much larger MFPs. $\kappa_{\rm ph}$ are dominated by phonons with MFPs below 100 nm. Half of the $\kappa_{\rm ph}$ are contributed from phonons with MFPs below 47 nm. These characteristic MFPs of electrons and phonons in Mo are similar to those in W [4]. However, Mo has much larger phonon MFPs but smaller electron MFPs than Al, Au and Ag [7]. The transport properties are reduced in nanostructures when the system size is comparable to the characteristic MFPs. In that regard, Mo nanostructures can be expected to show reduced Lorenz number.

IV. CONCLUSION

In this work, we derive the linearized phonon BTE accounting for ph-el scattering in addition to the

well-established ph-ph and isotope scatterings, and quantify the lattice thermal conductivity in elemental molybdenum. Mo has the same bcc structure as tungsten and similar phonon features including the triple degeneracy at high symmetry P and H points and the nearly isotropic phonon dispersion at long wavelengths. These features lead to weak ph-ph scattering at intermediate frequencies. As a consequence, $\kappa_{\rm ph}$ in Mo also possesses anomalous features including the large value, weak temperature dependence and increasing importance of exact solution of BTE with increasing temperature. Besides, Mo has a large isotope mixture and thus much stronger isotope scattering than W, consequently playing an important role in the thermal resistance. Furthermore, Mo has a weaker interatomic bonding than W, as revealed by the COHP analysis. Larger DOS at the Fermi level in Mo allows for more scattering channels, leading to slightly larger ph-el scattering. These three factors explain the smaller $\kappa_{\rm ph}$ of Mo despite of a lighter atomic mass. Considering the similarity of the phonon dispersion, our work suggests that another group-VI element chromium should also have a large $\kappa_{\rm ph}$, which accounts for the significant deviation of measured Lorenz number from the Sommerfeld value.

In addition, the calculated electrical conductivity of Mo agrees reasonably with the experimental data, especially around the room temperature. At high temperatures, the discrepancy between calculated and experimental results might be due to the unconsidered temperature effects in the DFT calculations. The calculated Lorenz number agrees with the Sommerfeld value L_0 within 7% for a wide temperature range. κ_e is not adequate to fully account for the measured total thermal conductivity, supporting the large calculated value of $\kappa_{\rm ph}$.

Mean free paths of electrons are also provided, determining the size effect of resistivity in nanostructures for applications such as interconnect. Furthermore, mean free paths of electrons are a few times smaller than those of phonons, suggesting that Lorenz numbers including the $\kappa_{\rm ph}$ contribution can be reduced in nanostructures.

ACKNOWLEDGMENTS

We acknowledge support from the Natural Science Foundation of China (NSFC) under Grant No. 11704258, the Shenzhen Science, Technology and Innovation Commission under Grant No. JCYJ20170412105922384, and the Natural Science Foundation of Guangdong Province under Grant No. 2017A030310377. J.M. acknowledges support from NSFC under Grant No. 11804229.

[1] C. Li, N. K. Ravichandran, L. Lindsay, and D. Broido, Phys. Rev. Lett. **121**, 175901 (2018).
[2] A. Kundu, J. Ma, J. Carrete, G. Madsen, and W. Li, Mater. Today Phys. **13**, 100214 (2020).
[3] Y. Chen, J. Ma, and W. Li, Phys. Rev. B **99**, 020305(R) (2019).
[4] Y. Chen, J. Ma, S. Wen, and W. Li, npj Comput. Mater. **5**, 98 (2019).
[5] J. Ma, W. Li, and X. Luo, Phys. Rev. B **90**, 035203 (2014).
[6] B. Liao, B. Qiu, J. Zhou, S. Huberman, K. Esfarjani, and G. Chen, Phys. Rev. Lett. **114**, 115901 (2015).
[7] A. Jain and A. J. H. McGaughey, Phys. Rev. B **93**, 081206(R) (2016).
[8] Y. Wang, Z. Lu, and X. Ruan, J. Appl. Phys. **119**, 225109 (2016).
[9] T. Wang, Z. Gui, A. Janotti, C. Ni, and P. Karandikar, Phys. Rev. Mater. **1**, 034601 (2017).
[10] Z. Tong and H. Bao, Int. J. Heat Mass Transfer **117**, 972 (2018).
[11] Z. Tong, S. Li, X. Ruan, and H. Bao, Phys. Rev. B **100**, 144306 (2019).
[12] S.-Y. Yue, R. Yang, and B. Liao, Phys. Rev. B **100**, 115408 (2019).
[13] L. Lindsay and D. A. Broido, J. Phys.: Condens. Matter **20**, 165209 (2008).
[14] A. Ward, D. A. Broido, D. A. Stewart, and G. Deinzer, Phys. Rev. B **80**, 125203 (2009).
[15] S.-i. Tamura, Phys. Rev. B **27**, 858 (1983).
[16] W. Li, Phys. Rev. B **92**, 075405 (2015).
[17] G. K. Madsen and D. J. Singh, Comput. Phys. Commun. **175**, 67 (2006).
[18] J.-J. Zhou and M. Bernardi, Phys. Rev. B **94**, 201201(R) (2016).
[19] T.-H. Liu, J. Zhou, B. Liao, D. J. Singh, and G. Chen, Phys. Rev. B **95**, 075206 (2017).
[20] J. Ma, A. S. Nissimagoudar, and W. Li, Phys. Rev. B **97**, 045201 (2018).
[21] S. Poncé, D. Jena, and F. Giustino, Phys. Rev. B **100**, 085204 (2019).
[22] P. B. Allen, Phys. Rev. B **17**, 3725 (1978).
[23] H. R. Schober and P. H. Dederichs, in *Phonon States of Elements. Electron States and Fermi Surfaces of Alloys Mo*, edited by K.-H. Hellwege and J. L. Olsen, in Landolt-Börnstein Vol. 13A of Group III (Springer-Verlag, Berlin Heidelberg, 1981).
[24] P. Giannozzi, S. Baroni, N. Bonini, M. Calandra, R. Car, C. Cavazzoni, D. Ceresoli, G. L. Chiarotti, M. Cococcioni, I. Dabo *et al.*, J. Phys. Condens. Matt. **21**, 395502 (2009).
[25] N. Troullier and J. L. Martins, Phys. Rev. B **43**, 1993 (1991).
[26] J. P. Perdew, K. Burke, and M. Ernzerhof, Phys. Rev. Lett. **77**, 3865 (1996).
[27] J. P. Perdew and Y. Wang, Phys. Rev. B **45**, 13244 (1992).
[28] S. Poncé, E. Margine, C. Verdi, and F. Giustino, Comput. Phys. Commun. **209**, 116 (2016).
[29] G. Kresse and J. Furthmüller, Phys. Rev. B **54**, 11169 (1996).
[30] G. Kresse and D. Joubert, Phys. Rev. B **59**, 1758 (1999).
[31] W. Li, J. Carrete, N. A. Katcho, and N. Mingo, Comput. Phys. Commun. **185**, 1747 (2014).
[32] W. Li, L. Lindsay, D. A. Broido, D. A. Stewart, and N. Mingo, Phys. Rev. B **86**, 174307 (2012).
[33] W. Li, N. Mingo, L. Lindsay, D. A. Broido, D. A. Stewart, and N. A. Katcho, Phys. Rev. B **85**, 195436 (2012).

[34] R. Dronskowski and P. E. Bloechl, J. Phys. Chem. **97**, 8617 (1993).
[35] S. Maintz, V. L. Deringer, A. L. Tchougreff, and R. Dronskowski, J. Comput. Chem. **37**, 1030 (2016).
[36] V. Singh, M. Kosa, K. Majhi, and D. T. Major, J. Chem. Theory Comput. **11**, 64 (2015).
[37] W. Li and N. Mingo, Phys. Rev. B **89**, 184304 (2014).
[38] A. Sparavigna, Phys. Rev. B **65**, 064305 (2002).
[39] A. Majumdar, J. Heat Transfer **115**, 7 (1993).
[40] W. M. Shaw and L. D. Muhlestein, Phys. Rev. B **4**, 969 (1971).
[41] J. F. Goff, Phys. Rev. B **1**, 1351 (1970).
[42] P. Klemens, in *Thermal Conductivity*, edited by R. P. Tye (Academic Press, New York, 1969), Vol. 1.
[43] P. D. Desai, T. K. Chu, H. M. James, and C. Y. Ho, J. Phys. Chem. Ref. Data **13**, 1069 (1984).
[44] J. Bass, in *Electrical Resistivity, Kondo and Spin Fluctuation Systems, Spin Glasses and Thermopower Hg - Nd*, edited by K.-H. Hellwege and J. L. Olsen, Landolt-Börnstein Vol. 15A of Group III (Springer-Verlag, Berlin Heidelberg, 1983).
[45] G. K. White, *Thermal Conductivity of Pure Metals and Alloys Ga - Pa*, edited by G. K. White and O. Madelung, in Landolt-Börnstein Vol. 15C of Group III (Springer-Verlag, Berlin Heidelberg, 1991).
[46] A. Giri, J. T. Gaskins, L. Li, Y.-S. Wang, O. V. Prezhdo, and P. E. Hopkins, Phys. Rev. B **99**, 165139 (2019).
[47] G. Daniel, J. Appl. Phys. **119**, 085101 (2016).